Supporting Information

Nanoscale Insight into Performance Loss Mechanisms in P3HT:ZnO Nanorod Solar Cells

Haian Qiu[1], Jong Hyun Shim[2], Junghyun Cho[2,3], Jeffrey M. Mativetsky[1,2*]

[1]*Department of Physics, Applied Physics, and Astronomy, Binghamton University, Binghamton, NY, 13902, USA*

[2]*Materials Science and Engineering Program, Binghamton University, Binghamton, NY, 13902, USA*

[3]*Department of Mechanical Engineering, Binghamton University, Binghamton, NY, 13902, USA*

*Email: jmativet@binghamton.edu

1. Photocurrent Density Calibration

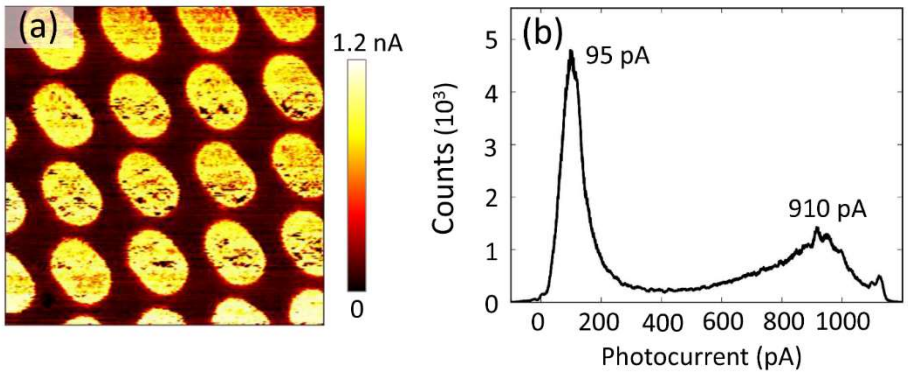

Figure S1. (a) Photocurrent map (10 µm x 10 µm) of a P3HT:ZnO nanorod active layer with micropatterned Au electrodes on top, measured under short circuit conditions (0 V) and 4.5 suns. The area of the micropatterned electrodes was measured to be 1.9 μm^2 (elongated shape due to evaporation geometry). (b) Corresponding photocurrent histogram showing two distinct peaks, one peak centered at 95 pA due to direct contact between the C-AFM probe and the active layer, and another peak at 910 pA due to C-AFM probe contact to the Au microelectrodes.

2. Piezo-Induced Current

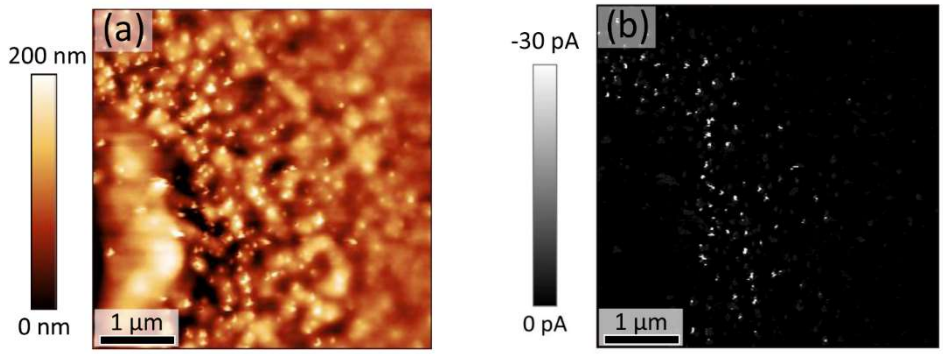

Figure S2. (a) Contact mode topography and (b) piezo-induced current map of a P3HT:ZnO nanorod sample with an incomplete P3HT coating, under short-circuit conditions (0 V) and 4.5 sun illumination (positive currents truncated at 0 pA). Negative piezo-induced current is clearly observed at locations where ZnO nanorods protrude.

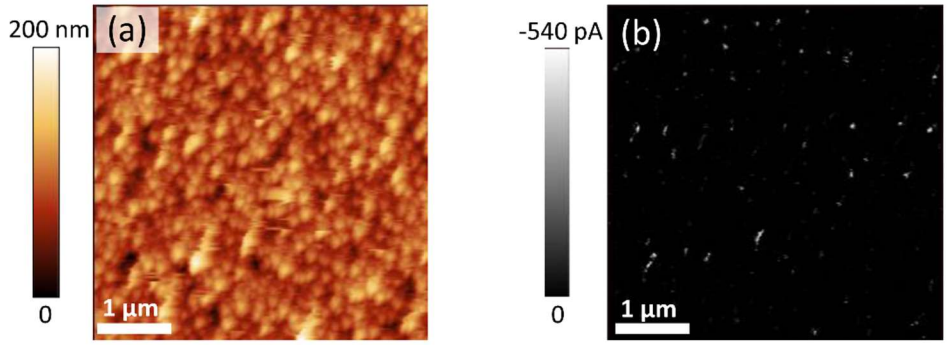

Figure S3. (a) Contact mode topography and (b) piezo-induced current map for a P3HT:ZnO nanorod sample with an incomplete P3HT coating, under short-circuit (0 V) and dark conditions (positive currents truncated at 0 pA).

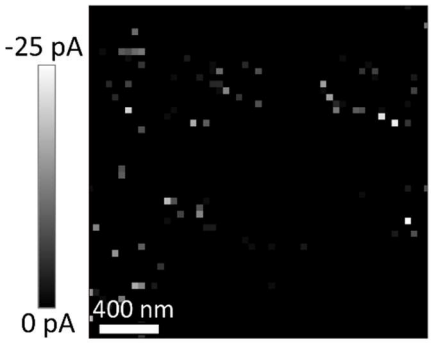

Figure S4. Negative piezo-induced current recorded during point-by-point current-voltage (PPIV) mapping of a P3HT:ZnO nanorod active layer under short circuit conditions and 4.5 sun illumination (sample area corresponds to Figure 4, 5 in main text, positive currents truncated at 0 pA). Piezo-induced currents were observed within the low-performance regions, indicating direct contact between the C-AFM probe and the ZnO nanorods within these regions.

3. Short-Circuit Current

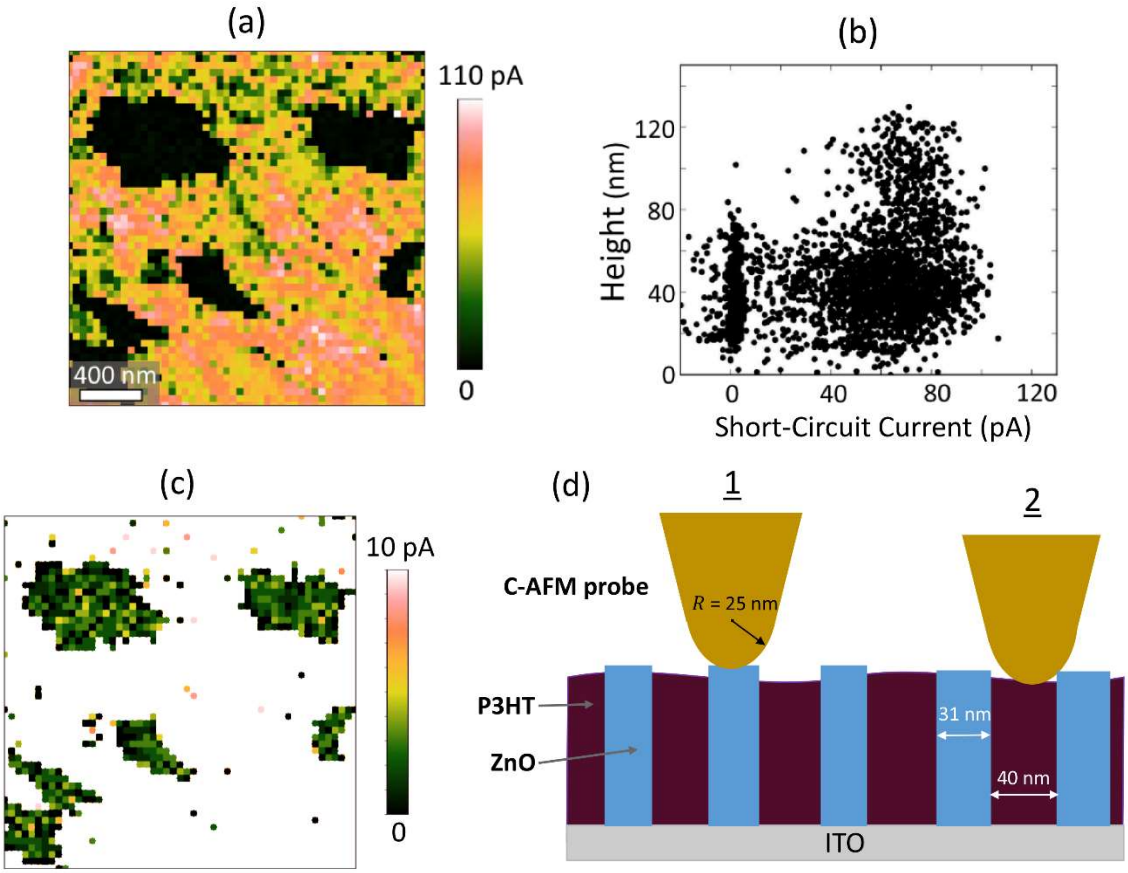

Figure S5. (a) Short-circuit current map of P3HT:ZnO nanorod active layer under 4.5 sun illumination (negative currents truncated at 0 pA). (b) Height versus short-circuit current scatter plot. (c) Truncated short-circuit current map with photocurrent ranging between 0 and 10 pA, showing small local photocurrent variations within the low-performance regions. (d) Schematic depicting the cause of current variations within low-lying regions. In case 1, the C-AFM probe makes direct contact with a nanorod, leading to piezo-generated current. In case 2, the probe makes contact with P3HT and a nearby nanorod simultaneously, resulting in the recombination of positive photocurrent and negative piezo-generated current.

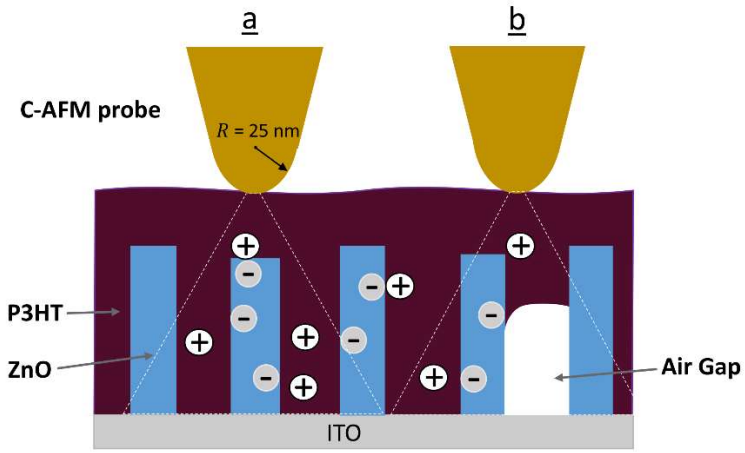

Figure S6. Schematic depicting (a) current spreading during C-AFM, and (b) current spreading near a buried air gap. The dashed lines represent the charge collection area which broadens at lower active layer depths. If a buried air gap were present, current spreading would lead to spatial averaging of the buried features and a gradual transition in measured current between high and low-performing regions.

4. Histograms

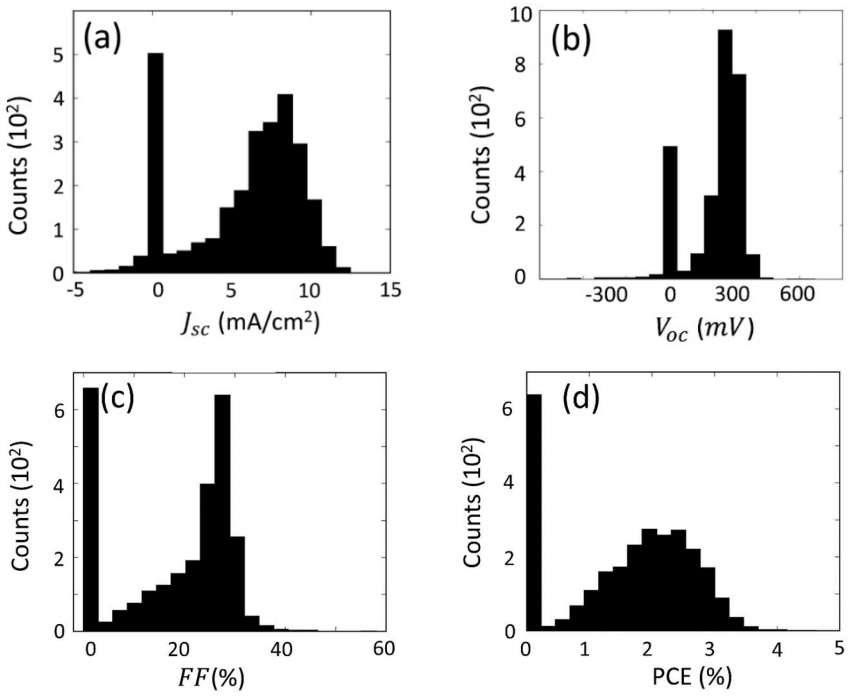

Figure S7. Histograms corresponding to Figure 4: (a) short-circuit current density under 1 sun illumination, (b) open-circuit voltage, (c) fill factor, and (d) power conversion efficiency.

5. Saturated Photocurrent

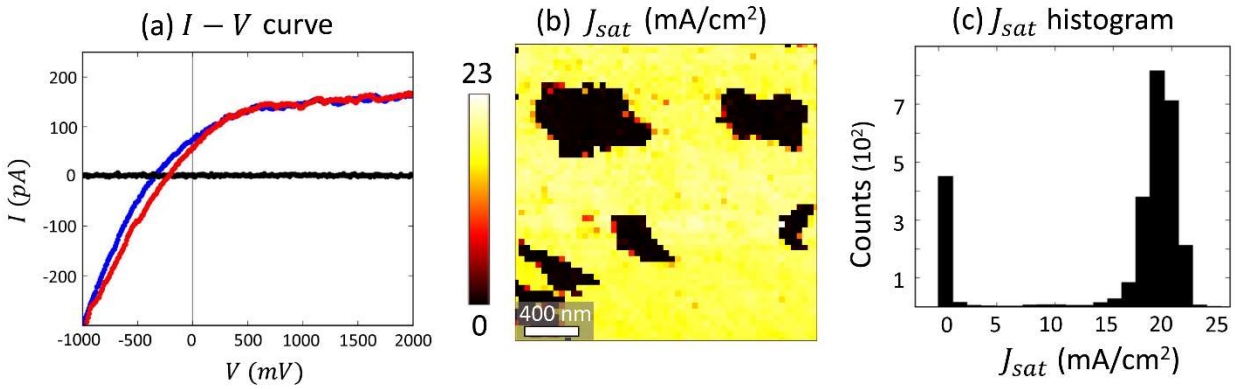

Figure S8. (a) Current-voltage curves showing saturated photocurrent at a reverse bias of +2 V, under 4.5 suns. (b) Saturated photocurrent density, J_{sat}, map at +2 V bias, estimated for 1 sun and (c) corresponding histogram with a peak value of 20 mA/cm^2. The photocurrent density distribution in (b) is uniform, except at the low-performance regions, where there is near-zero photocurrent (negative piezo-induced current truncated at 0 mA/cm^2).

6. Charge Collection Probability

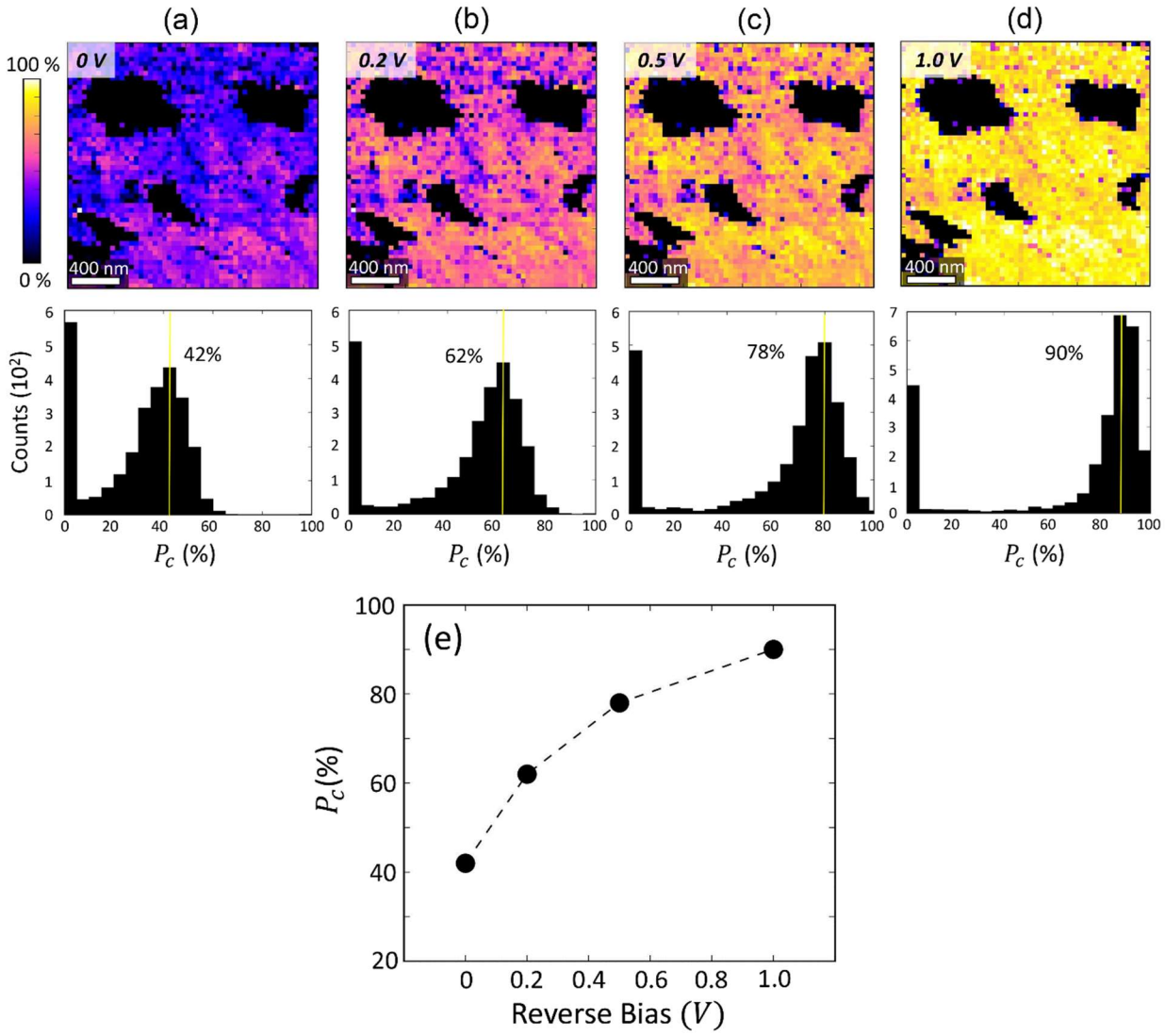

Figure S9. Mapped charge collection probability P_c as the reverse bias is varied: (a) 0 V, (b) 0.2 V, (c) 0.5 V, (d) 1.0 V. The corresponding histograms are shown beneath the P_c maps. (e) Charge collection probability peak values versus reverse bias. Charge collection probability increases as reverse bias increases and approaches 90% at +1 V.